ITALY – CANADA 2005
WORKSHOP ON:

"3D Digital Imaging and Modeling: Applications of Heritage, Industry, Medicine and Land"

17 – 18 May 2005

ORGANIZED BY:

Interdepartment Research Center in Cartography, Photogrammetry, Remote Sensing and G.I.S.

Università di Padova

C.I.R.GEO

FINAL PROGRAM

Provincia di Padova

Università degli Studi di Padova

Government of Canada
Gouvernement du Canada

Ambasciata del Canada

S1_3 ***Revolutional Constraints for Low-Cost 3D Scanning from Uncalibrated Images***
C. Colombo, D.Comanducci, A. Del Bimbo, F. Pernici
Department of Informatics Systems – University of Florence

S1_4 ***Numerical Analysis of Mutual Radiation Effects of Complex Surfaces***
G. Fanti – Department of Mechanic Engineering – University of Padua

S1_5 ***An Efficient Algorithm for 3D-Reconstruction in Cultural Heritage, Medicine and Industry***
M. Ioannides – CIPA Delegate Cyprus

S1_6 ***Investigation of Functional Response of Prosthetic System by Using Numerical Modeling***
A.N. Natali, G.P. Pavan, E.L. Carniel, A. Gasparetto – University of Padua
Centro Interdipartimentale di Ricerca di Meccanica dei Materiali Biologici

S1_7 ***Calibration of Thermal Imagery for Integration into 3D VR Models***
M. Gianinetto(*) F. Roncoroni(**), M. Scaioni(**)
(*) DIIAR, Polytechnic of Milano
(**) DIIAR, Center of Lecco, Polytechnic of Milano

S1_8 ***Symmetries and Topology for the Definition of Conceptual Models***
L. Mussio(*), D. Poli(**), A. Bozzoli(***)
(*) DIIAR, Polytechnic of Milano
(**) IGP ETH Zurich
(***) LIRIS – INSA de Lyon

13:00 – 14:30 *Lunch*

14:30 – 16:15 **Session 2**: *Computer Vision & Digital Photogrammetry*

Chair: Gianfranco Forlani (Italy)

S2_1 ***Stability Analysis and Potential Application of Amateur Digital Cameras***
A. Habib, A. Pullivelli
Department of Geomatics Engineering, University of Calgary

S2_2 ***Integrating Lidar Intensity Measures and Hyperspectral Data for Extracting of Cultural Heritage***
F. Coren(*), D. Visintini(**), G. Prearo(**), P. Sterzai(*)
(*) National Institute of Oceanographic and Experimental Geophysics, Trieste
(**) Department of Georisorse and Territorio- University of Udine

CALIBRATION OF CLOSE-RANGE THERMAL IMAGERY FOR INTEGRATION INTO 3D VR MODELS

M. Gianinetto [a], F. Roncoroni [b], M. Scaioni [b]

[a] Politecnico di Milano, DIIAR Rilevamento-Remote Sensing Lab, P.zza L. da Vinci 32, 20133 Milano, Italy
[b] Politecnico di Milano, DIIAR Rilevamento, Polo Regionale di Lecco, Via M. d'Oggiono 18/a, 23900 Lecco
e-mail: {marco.gianinetto, fabio.roncoroni, marco.scaioni}@polimi.it

KEY WORDS: Camera Calibration, Thermal Imagery, Cultural Heritage Documentation, Multi-Sensor Data Integration

ABSTRACT:

The appearance of terrestrial laser scanners (TLS) has provided a new data source of geometric information. Several TLS allow to be equipped by a calibrated camera, whose images may be directly mapped on the DSM as photo-texture. Here a further improvement is proposed, i.e. the integration of thermal imagery into the 3D model in order to acquire knowledge about internal stratigraphy of walls, floors, ceilings and other ancient structures. Obviously, a fundamental pre-requisite to obtain this task is the calibration of thermal sensor and the orientation of each image into the object reference system of the TLS data. Unfortunately, due to the poor radiometric and geometric quality of themal images, their integration into the TLS 3D model is a complex task; moreover, looking for control points which could be measured on both 3D model and thermal image is not trivial. This leads to the failure of methods performing calibration and orientation in a unique task, such as self-calibration approaches. Calibration has to be performed in laboratory. We have performed the calibration of a thermal camera NEC Thermotracer TH 7102 WX by means of a calibration dig and the computation of inner calibration in a bundle block l.s. adjustment. Data processing has been performed by using a low-cost photogrammetric commercial software.

1. INTRODUCTION

In the recent years the increasing development of new terrestrial sensors such as high resolution digital cameras, laser scanners, thermal cameras (TC) and geo-radars (GPR–Ground Penetrating Radars) have provided powerful tools for documentation and investigation in the architectural field. Although each kind of data yields specific information about the surveyed object, multi-sensor data integration has really open a new era. Traditionally, photogrammetry has been used for decades to describe architectural objects, but its derived products were substantially 2D line drawings. A key place in working methods which has taken place relates to the digital capture of data, resulting in a 3D output which can be easily managed by widespread CAD programs. On the other hand, rectified images and orthophotos have become of large application with the diffusion of soft-copy photogrammetric equipment and of digital cameras. Fusion of 3D object reconstruction and geometrically corrected images gave rise to photorealistic models, providing a new tools for visualization and cultural heritage documentation purposes.

The appearance of terrestrial laser scanners (TLS) has added a new powerful data source of geometric information. In a fast and simple way, a very dense point-cloud describing the surface (DSM) of an artifact can be captured. Thanks to interpolation methods, surfaces can be modelled to be used for deriving orthophotos as well. Furthermore, several TLSs allow to be equipped by a calibrated digital camera, whose images may be directly mapped onto the DSM as photo-texture.

In the same manner it is possible to use different sensors - such as TC or GPR - to collect data and to build photo-like textures.

In this paper we would like to deal with the problem of integrating laser scanning data and thermal imagery, in order to couple the representation of the object surface to that of its sub-surface. From a theoretical point of view, the same solutions adopted for mapping images onto a point cloud could be called for. Considering a laser scanner acquisition, this is usually georeferenced into a given reference system, which can be intrinsic to the instrument (*intrinsic reference system* – IRS) or may be related to the object; in the latter case, it is termed *project reference system* (PRS) or *ground reference system* (GRS) if it is geodetic. The image integration firstly requires its georeferencing in the same reference system the TLS data are. Three main strategies exist to do this:

1. the camera is mounted in a rigid way to the body of laser scanner, and its relative position with respect to the IRS is known from test-field calibration. In this case every captured image is already oriented in the point cloud, so that it can be straight-forward re-projected to create a photo-texture;
2. the camera is independent from the TLS, meaning that each image has to be registered into the reference system of laser data. Usually images to integrate to a point cloud are not captured in a block configuration, so that the solution for orientation is the use of a *space resection* algorithm based on the knowledge of enough ground control points (GCP);
3. images have been acquired by a block configuration, so that a global adjustment to register them into a given PRS is computed. Another chance is to perform a joint-adjusment comprehending either registration of scans and of images into a common PRS; a solution such this has been proposed by Ulrich *et al.* (2004). However, this approach is seldom used, at least up today.

When considering thermal cameras, several aspects must be accounted for to setup an integration process. First of all, this kind of camera cannot be mounted in a fixed position onto the TLS, because of different fields of view, different distances from the surface to be captured and the like. Details which appear in thermal cameras are points featuring a high contrast due to sharp differences of temperature. This means that trying

to identify corresponding points in the point cloud and then in the thermal imagery is quite difficult, even though colour digital images already mapped might help. Furthermore, thermal camera are usually equipped by lens featuring strong distortion that has to be compensated for. The method to register each thermal image in the RS of the point-cloud (but the problem would be the same in case of integration into a photogrammetric block) relies on computing a space resection, encompassing also the estimation of parameters for internal camera calibration as well. Disregarding some other aspects such has the numerical stability of the solution, such a method would require several GCPs, making the georeferencing a complex procedure. In order to simplify this task, we have chosen the approach which is commonly used with digital camera, i.e. the preliminary compution of intrinsic camera calibration parameters to be used as fixed values in the exterior orientation algorithms. However, this task is not trivial when it is applied to thermal cameras, because different specific problems give rise, as shown in par. 2. In the following of the paper a practical solution to computing the calibration of a thermal camera is proposed, by describing the setup of a test-field for data acquisition, and by describing an experience concerning a NEC Thermotracer TH 7102 WX thermal sensor. Furthermore, some tests finalized to evaluate the accuracy of the computed parameters has been done. In the selection of the strategy adopted to perform the calibration process, large importance has been focused on its reproducibility by non photogrammetrist operators as well. For this reason, a widespread used low-cost photogrammetric SW has been used and some guidelines to carry out the whole process given.
The structure of the paper is based first on the description of thermal sensors features, with particular enphasis on their geometrical aspects. Then the adopted procedure for TC calibration is described and its application to NEC Thermotracer TH 7102 WX reported.

2. OVERVIEW OF THERMAL CAMERAS

2.1 Thermal cameras

Thermal imaging devices, widely used in modern medicine and especially in sport medicine, are today being used for non-invasive and non-destructive testings on buildings and historic structures. *Infrared thermography* (IRT) is a non-destructive and non-contact technique based on the measurement of the heat energy and its conversion into an electrical signal which is turned into a thermal digital image by a microprocessor (Capizzi *et al.*, 2004).
The efficiency of IRT as a non-destructive technique is well documented in many fields of engineering and in investigation of historical structures, where a restoration or conservation treatment might cause irreversible damage to the structure (Avdelidis *et al.*, 2004). In the civil engineering and in architecture IRT can be successfully used as an alternative to conventional inspection technologies to detect subsurface defects and hidden structures in wide areas (Binda *et al.*, 2003). Moreover, IRT is complemented by other non-destructive techniques such as GPR or sonic measurements.
Advantages of using IRT in the structural analysis of ancient buildings are mainly related to the low cost and high productivity of possible investigations. Infrared thermography can be divided into two different approaches: *passive IRT* and *active IRT*. In the *passive* approach, materials and structures are sensed at ambient temperature and anomalous temperature profiles or hot spots indicate a potential problem to take care of. In the *active* approach an external stimulus is used to induce a relevant thermal contrast naturally not present. Depending on the external stimulus applied, different methods have been developed, such as *pulse thermography*, *step heating*, *lockin thermography*, *burst-phase thermography* or *vibro-thermography*: a review about these technologies can be found in Maldague (2000 and 2002).
Standard active thermograph techniques such as *lockin thermography* or *burst-phase thermography* apply only temporal varying patterns to the surface of the object to be investigated. As a consequence, the heat flow is basically directed perpendicularly to the surface. In contrast, spatially varying heat flow applied to surfaces detect also temperature differences parallel to the surface and thus it is also sensitive to lateral conductivity changes (Jähne, 2004).
Interpretation of *pulse thermography* data sequences has typically been based on the contrast analysis, in which regions with subsurface anomalies are visually identified with respect to defect-free areas. The derivative images offer an extremely clear visualization of subsurface features, and in many cases it is possible to detect features in derivative images that are totally undetectable in normal contrast images. The derivative images offer a high degree of immunity to non-uniform heating and display less blurring than contrast images, as features may be detected earlier, before that significant lateral diffusion occurs (Shepard *et al.*, 2004).
Regarding the *mechanical vibrations induced* technique (*vibro-thermography*), ultrasound excited thermography allows for defect selective imaging using thermal waves that are generated by elastic waves. The mechanism involved is a local friction which turns a dynamically loaded defect (for example a crack) into a heat source which is identified by the thermographic system (Zweschper *et al.*, 2004).

2.2 Geometric aspects of thermal imagery

A *thermogram* (thermal image) can be seen as a matrix where the row and column pixel coordinates are related to the planimetric position of the sensed detail and the value represent the pixel temperature. The focal plane array (FPA) of a thermal camera typically has a small format (e.g. 320x240 pixel). This means that using a standard optics with a narrow field of view (FOV) of 29° horizontal and 22° vertical, at a distance of 10 m from the target, the pixel size of the thermogram is about 2.5 cm^2. This is a low resolution if compared to those of other terrestrial sensors used in engineering and architectural surveying field (e.g. photogrammetric digital cameras or TSLs). Moreover, infrared thermal cameras have been widely used as qualitative and quantitative radiometric inspecting instruments but the geometric quality of the data has not been deeply investigated. Typically, thermographic data and their numerical processing are represented in the image reference system which may be affected by high geometric deformations as well. It follows that the location of phenomenon studied may be poorly identified.
This aspect turn out to be very important when the IRT is not treated as a stand alone technique but becomes an informative layer which should be fused with different data to build up 3D models. In this case, thermal images must be rectified and thus it is necessary the knowledge of camera calibration (principal distance, location of the principal point and lens distortion).
In the following paragraph the calibration process of a thermal camera is addressed to. In this case, its application has regarded the specific NEC Thermotracer TH 7102 WX thermal sensor, but it could be generalized in order to be used with other models as well.

3. A STRATEGY FOR THE GEOMETRIC CALIBRATION OF A THERMAL CAMERA

3.1 Some critical aspect of thermal cameras calibration

From a theoretical point of view the most part of current thermal cameras follow the perspective model, so that their calibration could be performed by the standard approach usually applied for close-range digital cameras (see Aoyama & Chikatsu, 2004). On the other hand, from a practical point of view several problems arise, which are mainly due to the followings items:

- large lens distorsion;
- large pixel size, making difficult the collimation of details in imagery;
- small image format;
- high sensitivity to variations of surface temperature and low sensitivity to variations in surface radiometric reflectivity;
- cameras are usually equipped by an autofocus device which cannot be turned off;
- reduced information about the internal sensor geometry (in many countries – e.g. in the United States – thermal cameras are considered as a technology of militar interest and then protected).

The combination of these factors make calibration a not trivial task. In order to investigate this field, we have performed a test finalized to the calibration of a NEC Thermotracer TH 7102 WX thermal camera. This sensor has been already used by the authors to acquire imagery for analysis of the sub-surfaces of some ancient buildings. Its application has yielded very satisfying results when thermal imagery have been used as stand alone data. On the contrary, difficulties have appeared when integration to other laser scanners and photogrametric data has been tried. In order to overcome these problems, the decision to perform the camera calibration has been taken.

3.2 Termovision system description

Calibration tests have been performed for the NEC Thermotracer TH 7102 WX thermal camera. This sensor is equipped by an uncooled micro-bolometric focal plane array operating in the 8-14 μm spectral region with standard thermal measuring range varying from -40° to +120°. The temperature resolution is 0.08° at 30°. The size of the images is 320x240 pixels, with a FOV of 29° (H) x 22° (V) and an instantaneous field of view (IFOV) of 1.58 mrad. In Table 1 all main features of the camera are presented, while in Fig. 1 a picture is reported.

3.3 Calibration polygon setup

In order to perform the camera calibration, a polygon made up of a set of GCPs has been established, so that a full field-calibration could be performed. The geometric layout of the polygon is depicted in Fig. 2, showing the disposal of 40 GCPs in the xy plane. Each GCP is materialized by a hiron nail fixed on the wooden plane framework; the length of nails varies from 3 up to 6 cm in z direction from the basement plane. A prototipe of such a polygon has been built in laboratory and fixed to an external wall in vertical position (see Fig. 3). This location has simplified the measurement of GCP coordinates by a total station, which has been stationed in 3 positions in front of the polygon. All 3D coordinates of GCPs have been computed from intersection of angular measurements with an accuracy in the order of ±2 mm.

The acquisition of thermal images has been carried out by applying a standard block configuration usually adopted for digital camera calibration. As can be seen in Fig. 4, the block is made up of 13 images, comprehending 8 images captured from up, down, left and right directions with the camera body in both vertical and horizontal position; 4 images have been acquired from diagonals and 1 from nadir direction. Being impossible to disactivate the autofocus device, all images have been approximately taken from the same distance to the polygon center, following the layout depicted in Fig. 5. Three blocks of images have been captured, respectively at a mean distance of 3, 4 and 5.3 m.

To improve the visibility of nails used as GCPs in thermal imagery, they have been warmed up just before data capture. This solution has allowed to acquire images with well contrasted targets with respect to the wooden background, as can be shown in figure 6.

Measuring range	Standard 1: -40° ÷ +120° Standard 2: +0° ÷ +500°
Thermal resolution	0.08° at 30°
Spectral range	8-14 μm
FOV	29° (H) x 22° (V)
IFOV	1.58 mrad
Focusing range	50 cm to infinity
Image resolution	320 (H) x 240 (V) pixel
Quantization	14-bit

Table 1 - NEC Thermotracer TH 7102 WX specifications

Figure 1 - A picture of the NEC Thermotracer TH 7102 WX thermal camera

3.4 Estimation of calibration parameters

This task has been performed by applying the commercial photogrammetric SW PhotoModeler 4.0 (EOS Systems Inc.). The selection of a commerical SW has been done in order to setup a calibration procedure that could be easily repeated also by non photogrammetrists.

PhotoModeler is provided by a module for digital camera calibration, task that can be carried out by the acquisition of some photos of a pre-defined test-field. Here we could not apply this procedure, due to the fact that images of test-field do not result enough contrasted to guarantee a precise measurement of control points. Then each block (made up of 13 images) of the calibration polygon described at par. 3.3 has been solved in a bundle adjustment with additional parameters.

All targets have been measured on all photos where they are imaged and used as fixed GCPs.
In the following sub-paragraphs some aspects of block orientation are presented, while in next par. 4 numerical results are shown.

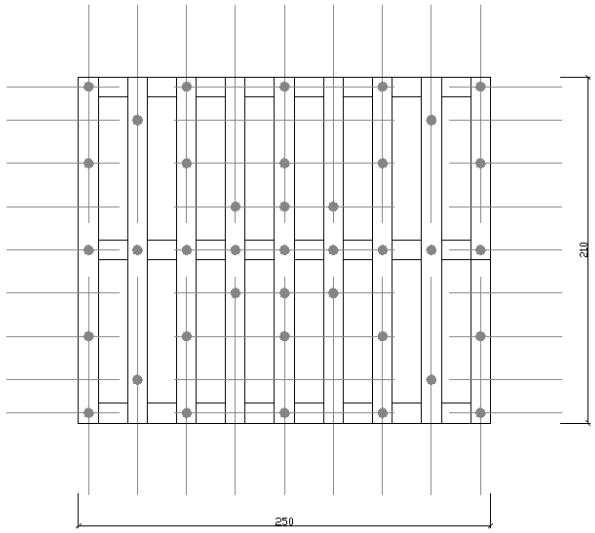

Figure 2 - Calibration polygon layout (size in m)

Figure 3 - First prototype of the GCPs polygon developed for the geometric calibration of thermal cameras

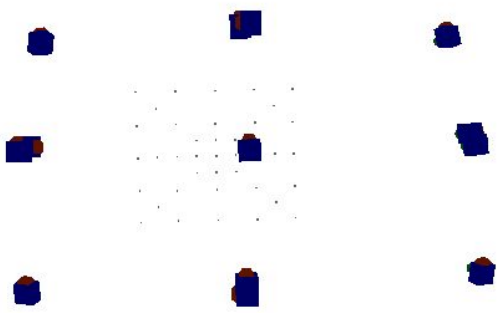

Figure 4 - Configuration of each block used in camera calibration

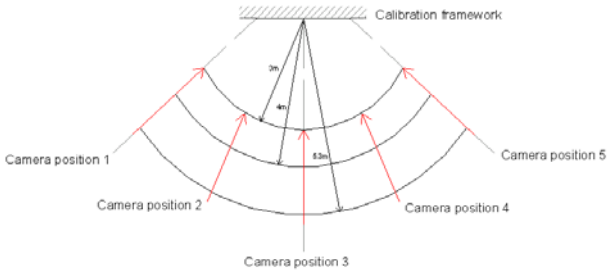

Figure 5 - Geometrical layout of camera positions with respect to the GCP polygon

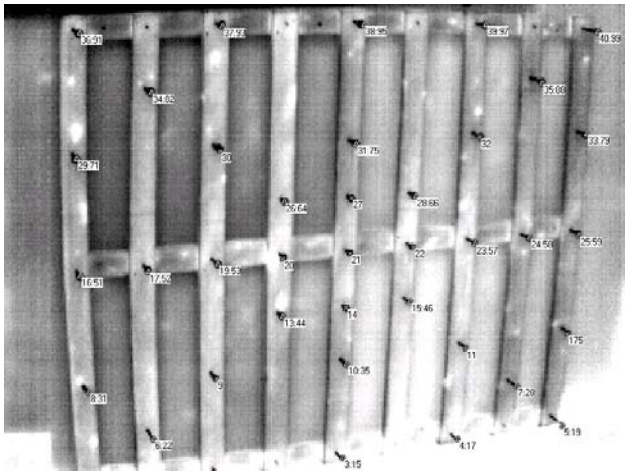

Figure 6 - Thermal image of the calibration polygon with superimposed the measures of GCPs

3.4.1 Approximation of parameters. The adopted SW do not require any approximation for exterior orientation parameters, that are needed on the contrary for interior orientation. The geometric model implemented is based on the following set of parameters:

- principal distance (c);
- coordinates of principal point (x_0,y_0);
- coefficients to compensate for radial lens distortion (K_1,K_2);
- coefficients to compensate for tangential lens distortion (P_1,P_2).

Estimation of these parameters adds up 7 unknowns to the l.s. bundle block adjustment. The algorithm implemented in PhotoModeler to compute this task needs at least 8 GCPs which can be measured on all the block images. This condition has been widely satisfied for blocks at 4 and 5.3 m, while has not for the block at 3 m. In the last case, images covered only the central portion of the framework, resulting in few GCPs available for the orientation.
In the technical specification of Thermotracer TH 7102 WX camera no information about the physical size of the sensor is given, being the image size in pixel the mere available data (Table 1). To overcome this problem, a conventional sensor size has been setup and the other parameters scaled with respect to this (6.8452 x 5.1586 mm).
Concerning initial values for others parameters, principal distance has been computed from measuring some distances

between GCPs in the nadir image. The initial principal point position has been selected in the middle of the sensor, while for all distortion coefficients the naugh value has been assigned.
Thank to these approximations the solution has been estimated for the block taken at 5.3 m from the polygon. Secondly, the solution of the block at 4 m has been found by starting from the set of parameters computed for the other block.

3.4.2 Workflow of the calibration procedure. The computation of block orientation with included calibration parameters has followed the usual general workflow adopted in photogrammetric block adjustment, made up of image selection and preparation stage, measurement of image coordinates of GCPs and computation of bundle adjustment. However, the PhotoModeler software allows to use some tools which may help the user to perform different processing tasks and to reduce the work to do. For this reason we report in the following the workflow of the adopted calibration procedure:

1. *project setup*: input of GCP coordinates, initial values for camera calibration parameters, selection of photos to be used;
2. *manual measurement of GCP image coordinates*: the centre of each nail used as GCP has been measured by manual collimation; unfortunately, no automatic algorithm for control point measurement could be applied, because the basement of nails would have introduced a bias in the measurement. At this stage point have been measured but have not been labelled yet;

3. *manual labelling of 6 GCPs per image*: in order to computing a first stable orientation for the block, a small set of geometrically well distributed GCPs is labelled on all the images;

4. *computation of initial exterior orientation*: each image is oriented by space resection based on the set of labelled GCPs; in a second stage, a first bundle adjustment is computed without including the estimation of calibration parameters;

5. *automatic labelling of remaining GCPs*: thank to the computed orientation, all the other GCPs are now labelled by exploiting epipolar constraints; the searching for corresponding points require the definition of a threshold depending on the accuracy of estimated orientation; in the calibration polygon GCPs have been positioned quite far from each to other, in order to avoid wrong correspondencies; eventually, missing points are integrated by manual labelling;

6. *bundle block computation with estimation of calibration parameters*: the final orientation is computed in two steps, the first without including calibration parameters to detect possible gross errors in image point measurements, the second to get the estimation of calibration parameters as well.

In the following par. this procedure applied to both considered blocks is described.

4. NUMERICAL RESULTS

The calibration has been computed separately for each block at 4 and 5.3 m blocks, because the autofocus device results in a change of focal length. Main characteristics of both blocks are reported in Table 2, while results of calibrations are in Table 3.
Not negligible differences appear between results obtained from both blocks, especially in parameter c and x_0. In both cases, high correlations (>80%) have resulted between parameters x_0 and P_1. However, from the direct analysis of estimated parameters and their st.dev.s it is very difficult to find any conclusions about the quality of results. In order to do this, some further tests have been tried.

4.1 Analysis of the accuracy of estimated calibration parameters

The first test that has been leaded to assess the quality of calibration has concerned the recomputation of a bundle adjustment of the same blocks, by fixing at this stage the estimated calibration parameters and by using a small set of GCPs (5) as constraints.
Barring nails that have been still used as GCPs, all other have played as *tie points* (TPs) in the bundle adjustment. Coordinates of TPs computed after the adjustment have been compared to their reference values determined by topographic measurements. Results in term of R.M.S. of differences are reported in Table 4, where also R.M.S. of l.s. estimation of st.dev.s can be seen. Computed R.M.S. have resulted slightly better then the expected theoretical values. Furthermore, it can be noticed that the mean values of differences has resulted near 0 for both blocks, meaning the absence of systematic effects.
The fact that theoretical and practical results have resulted better for the block at 5.3 m with respect to the other reveals the importance of a good geometric configuration for the images of the block to be used for computing camera calibration.
A further test has been performed on the 5.3 m block only, by fixing the same 5 GCPs used previously and by considering at this time all TPs as independent check points (these has not been used as tie points for computing the bundle adjustment) and by adopting the estimated camera calibration parameters in Table 3. In this case results in term of R.M.S. of differences computed on independent check points (see Table 4) have resulted slightly worse than in the previous test, but however in the order of the pixel size of Thermotracer TH 7102 WX camera, which is about 1.2 cm on the ground at a distance of 5 m.

block	**"4 m"**	**"5.3 m"**
# of images	13	13
# of GCPs used	35	39
# of GCPs imaged on all photos	16	21
mean # of GCPs per image	23	33
mean # of rays per 3D point	9	11

Table 2 – Main features of both blocks used for camera calibration.

camera param.s	block "4 m"		block "5.3 m"	
	mean	*st.dev*	*mean*	*st.dev*
c [mm]	13.4276	±0.133	13.0566	±0.155
x_0 [mm]	3.6059	±0.195	3.4906	±0.152
y_0 [mm]	2.8942	±0.173	2.8565	±0.153
K_1	$3.634 \cdot 10^{-3}$	$\pm 6.0 \cdot 10^{-4}$	$2.777 \cdot 10^{-3}$	$\pm 6.3 \cdot 10^{-4}$
K_2	$1.068 \cdot 10^{-5}$	$\pm 3.4 \cdot 10^{-5}$	$8.351 \cdot 10^{-5}$	$\pm 3.8 \cdot 10^{-5}$
P_1	$2.741 \cdot 10^{-4}$	$\pm 3.7 \cdot 10^{-4}$	$-6.278 \cdot 10^{-5}$	$\pm 3.4 \cdot 10^{-4}$
P_2	$-1.117 \cdot 10^{-3}$	$\pm 3.9 \cdot 10^{-4}$	$-6.849 \cdot 10^{-4}$	$\pm 3.6 \cdot 10^{-4}$

Table 3 – Estimated camera calibration parameters and their standard deviations.

		block "4 m"	block "5.3 m"
# of GCPs		5	5
# of ICPs		31	34
theoretical RMS on TPs	***X [mm]***	16	4
	Y [mm]	8	3
	Z [mm]	22	9
computed RMS on TPs	***X [mm]***	5	2
	Y [mm]	7	3
	Z [mm]	6	5
computed RMS on ICPs	***X [mm]***	-	7
	Y [mm]	-	5
	Z [mm]	-	14

Table 4 – Results of tests with TPs and independent check points (ICP).

5. CONCLUSIONS

In this paper a procedure for calibrating a thermal camera Thermotracer TH 7102 WX has been proposed. The methodology has been applied to a specific camera, but it could be repeated by considering other models which would be based on the perspective geometry.

The adopted strategy consisted in three main stage: bulding up of a calibration polygon with a sufficient number of GCPs, acquisition of the images by the thermal camere, and l.s. block adjustment to estimate the camera calibration parameters.

All the procedure has been performed by means of a commercial low-cost photogrammetric software in order to demonstrate the possibility of applying this procedure by non photogrammetrists as well.

The accuracy of camera calibration, assessed by some quality tests, has resulted in the same order of the pixel size.

AKNOWLEDGEMENTS

The authors would like to thank Prof. Alberto Giussani (Politecnico di Milano – Polo Regionale di Lecco) for the support to this research. Thanks go to Prof. Bortolino Saggin (Politecnico di Milano – Polo Regionale di Lecco) for providing the thermal camera Thermotracer TH 7102 WX used in tests. Finally aknowledgements go to the student Antonino Nicastro who cooperate to this work during its degree thesis at Politecnico di Milano.

REFERENCES

References from Books:

Maldague, X., 2000. Applications of Infrared Thermography in NonDestructive Evaluation. In Pramod Rastogi (ed.), *Trends in Optical Nondestructive Testing*, pp. 591- 609.

References from Journals:

Maldague, X., 2002. Introduction to NDT by Active Infrared Thermography. *Materials Evaluation*, n. 6(9), pp. 1060-1073.

References from Other Literature:

Aoyama, K., and Chikatsu, H., 2004. Efficient calibration of amateur digital camera and orientation for photogrammetric applications. *The Int. Archive of the Photogrammetry, Remote Sensing and Spatial Information Sciences*, Vol. 35, Part B, pp. 382-387.

Avdelidis, N.P., Moropoulou, A. and Delegou, E.T., 2004. A thermographic study for the assessment of historic structures. In *Proc. of 7th Int. Conf. on Quantitative Infrared Thermography*, July 5-8, von Karman Institute, Rhode-St-Genèse, Belgium.

Binda, L., Lualdi, M., Saisi, A., Zanzi, L., Gianinetto, M. and Roche, G., 2003. NDT applied to the diagnosis of historic buildings: a case history. In *Proc. of the Int. Conf. on Structural Faults and Repair*, 1-3 July, London, pp. 10, on CD-ROM.

Capizzi, P., Cosentino, P., Fiandaca, G., Messina, P. and Terranova, L., 2004. Structural investigations by infrared thermography and SPR. In *Proc. of the 1st Int. Conf. of Applied Geophysics for Engineering*, Oct. 13-15, Messina, Italy.

Jähne, B., 2004. Spatiotemporal Active Thermography. In *Proc. of 7th Int. Conf. on Quantitative Infrared Thermography*, July 5-8, von Karman Institute, Rhode-St-Genèse, Belgium.

Shepard, S.M., Lhota, J.R., Hou, Y., Wang, D. and Ahmed, T., 2004. Reconstruction and Analysis of Pulsed Thermographic Data. In *Proc. of 7th Int. Conf. on Quantitative Infrared Thermography*, July 5-8, von Karman Institute, Rhode-St-Genèse, Belgium.

Ullrich, A., Schwarz, R., and H. Kager, 2003. Using Hybrid Multi-Station Adjustment for an Integrated Camera Laser-Scanner System. In Proc. of *Optical 3D Meas. Tech. VI*, Zurich, pp. 298-304.

Zweschper, T., Riegert, G., Dillenz, A. and Busse, G., 2004. Ultrasound Excited Thermography - Advances Due To Frequency Modulated Elastic Waves, In *Proc. of 7th Int. Conf. on Quantitative Infrared Thermography*, July 5-8, von Karman Institute, Rhode-St-Genèse, Belgium.